DOI: 10.1002/asia.200600293

Manipulating the Through-Space Spin–Spin Interaction of Organic Radicals in the Confined Cavity of a Self-Assembled Cage

Koji Nakabayashi,[a] Masaki Kawano,*[a] Tatsuhisa Kato,[b] Ko Furukawa,[c] Shin-ichi Ohkoshi,[d] Toshiya Hozumi,[d] and Makoto Fujita*[a]

Abstract: We show a new approach to manipulating the through-space spin–spin interaction by utilizing the confined cavity of a self-assembled M_6L_4 coordination cage. The coordination cage readily encapsulates stable organic radicals in solution, which brings the spin centers of the radicals closer to each other. In sharp contrast to the fact that the radical in solution in the absence of the cage is in a doublet state, in the presence of the cage through-space spin–spin interaction is induced through cage-encapsulation effects in solution as well as in the solid state, resulting in the triplet state of the complex. These results were confirmed by ESR spectroscopy and X-ray crystallography. The quantity of triplet species generated by encapsulation in the cage increases with increasing affinity of the radicals to the cage. We estimated the affinity between several types of guests and the cage in solution by cyclic voltammetry. We also demonstrate that the through-space interaction of organic radicals within the self-assembled coordination cage can be controlled by external stimuli such as heat or pH.

Keywords: EPR spectroscopy · host–guest systems · palladium · radicals · self-assembly

Introduction

Since the discovery of ferromagnetism in an organic radical in 1989, organic radicals and metal complexes have attracted considerable attention because they are promising in the development of molecule-based magnetic materials and devices, which have flexible designs based on organic synthesis.[1] Recent reports have revealed intriguing characteristics of organic radicals such as magnetic bistability and photoresponsive magnetism.[2] One of the most-important tasks in developing organic magnets is to induce spin–spin interaction by a "through-bond" or "through-space" approach. The through-bond approach has been intensively studied and developed because it can produce ferromagnetic spin–spin interaction much more easily than the through-space approach.[3] Furthermore, the through-space spin–spin interaction, which is proportional to $1/r^3$ (r = spin–spin distance), is ordinarily very weak and does not work effectively because bulky functional groups attached beside the spin center of a stable radical stop the spin centers from being spontaneously close to each other.[1,4] Therefore, spin centers need to be restrained by chemical bonds to produce spin–spin interaction. However, the through-bond approach is inflexible in designing and preparing magnetic molecules and in switching the magnetic interactions.

Numerous metal complexes, especially cyano-bridged complexes, have been synthesized and studied because spins on metals can readily interact with each other by super-exchange interaction through cyano groups to induce bulk magnetism effectively.[5] Magnetism responsive to external stimuli such as photoexcitation and humidity was later discovered.[6] Recently, magnetism of host–guest systems con-

[a] K. Nakabayashi, Prof. Dr. M. Kawano, Prof. Dr. M. Fujita
Department of Applied Chemistry
Graduate School of Engineering, University of Tokyo
CREST (Japan) Science and Technology Corporation (JST)
Bunkyo-ku Tokyo 113-8656 (Japan)
Fax: (+81) 35-841-7257
E-mail: mkawano@appchem.t.u-tokyo.ac.jp
mfujita@appchem.t.u-tokyo.ac.jp

[b] Prof. Dr. T. Kato
Department of Chemistry
Faculty of Science, Josai University
1-1 Keyakidai Sakado Saitama 350-0295 (Japan)

[c] Dr. K. Furukawa
Institute for Molecular Science
The Graduate University for Advanced Studies
Myodaiji, Okazaki 444-8585 (Japan)

[d] Prof. Dr. S.-i. Ohkoshi, Dr. T. Hozumi
Department of Chemistry
Graduate School of Science, University of Tokyo
Bunkyo-ku Tokyo 113-8656 (Japan)

Supporting information for this article is available on the WWW under http://www.chemasianj.org or from the author.

sisting of host metal complexes and guest molecules such as water, alcohol, and small aromatic molecules has begun to draw attention because the magnetism can be tuned by guest exchange.[7]

In contrast with the guest-tuneable magnetism of coordination-complex systems mentioned above, we report herein the induction of spin–spin interaction between organic radicals by using self-assembled coordination cages. Prior to this work, we demonstrated the encapsulation of organic molecules, the stereoselective transformation of the guests, and the stabilization of labile species within coordination cages.[8] In this article, we report that self-assembled cages **1a** and **1b** encapsulate organic radicals **2**–**5**, which have no

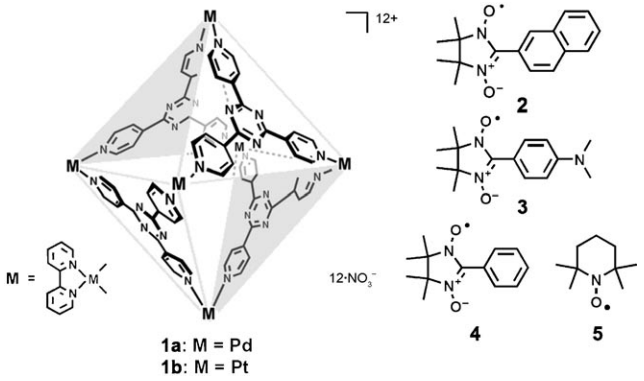

particular intermolecular interactions in solution, to form stable host–guest complexes and induce the triplet state. The radical centers of the guests are forced to be close to each other within the cavity of cages. As a result, through-space interaction between the two organic radicals is observed even in solution. Moreover, we show that the interaction can be controlled by external stimuli such as heat and pH. Preliminary results with radicals **2** and **3** have been previously reported.[9]

Abstract in Japanese:

空間を介したスピン間の相互作用を制御することは柔軟なスピン材料を設計するうえで重要である。自己集合性かご状錯体を用いることで有機安定ラジカル分子間でのスピン-スピン相互作用が制御可能になった。複数個のラジカル分子はお互いのスピン中心を近づける形でかご状錯体内に複数個取り込まれる。それにより錯体内のラジカル分子は相互作用し三重項状態が誘起される。水溶液中でもラジカル分子はかご状錯体内に包接されているため、固体状態のみならず水溶液中でも三重項状態は観測された。また溶液中で誘起される三重項状態とかご状錯体とラジカル分子の親和力との関係をサイクリックボルタンメトリーにより確認した。親和力を制御する因子として熱やpHを用いることでこの三重項状態の外部刺激による制御が可能になった。以上の結果はESRスペクトル、X線結晶構造解析およびUV-visスペクトルにより確認された。

Results and Discussion

Preparation of Host–Guest Systems

The self-assembly of cages **1a** and **1b** and their host properties have been previously described.[10] A series of clathrate compounds **1a**·(**2**)$_2$, **1b**·(**3**)$_2$, **1a**·(**4**)$_2$, and **1a**·(**5**)$_4$ were readily prepared by suspending an excess of powdered guest in the solution of a cage at 293 K for 1 h. The driving force of encapsulation is hydrophilic interaction between the cage and the guest. Single crystals of all the clathrate compounds suitable for X-ray analysis were obtained by slow evaporation of the solution. The host–guest stoichiometries were confirmed by elemental analysis.

Radical **2** encapsulated in **1a** in H_2O showed a broad absorption band at 650 nm accompanied with vibronic coupling (Figure 1), whereas no vibronic coupling was observed in the absence of **1a** (Figure S1). Vibronic coupling in **2** was also observed in acetone in the absence of **1a**. Therefore,

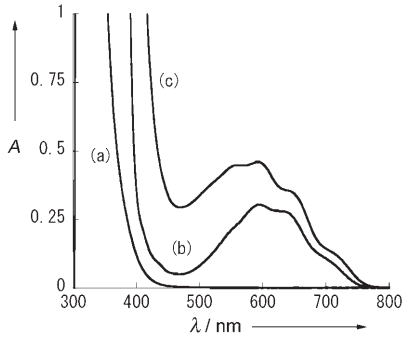

Figure 1. UV/Vis spectra of a) a solution of **1a** in 5 mM H_2O, b) a solution of **2** in 10 mM acetone, and c) a solution of **1a**·(**2**)$_2$ in 5 mM H_2O at 293 K.

the presence of vibronic coupling even in H_2O (Figure 1c) indicates that the radicals are present in the hydrophobic cavity of **1a**. Vibronic coupling was observed in **1b**·(**3**)$_2$ as well (Figure 8a).

Crystallographic Study

The crystal structures of **1a**·(**2**)$_2$, **1b**·(**3**)$_2$, **1a**·(**4**)$_2$, and **1a**·(**5**)$_4$ were determined by X-ray diffraction with a SMART CCD area detector diffractometry system. Crystallographic analyses clarified that guests **2**, **3**, and **4** are encapsulated at specific positions within the cage. The hydrophobic functional groups, such as naphthyl, aminophenyl, and phenyl groups, face the hydrophobic interior of the cage (Figure 2). Notably, the spin centers about the nitronyl nitroxide groups[11] of these radicals in the cage are considerably closer to each other than those in the guest crystals. The average intermolecular distances between the nearest and farthest spin centers are 5.9, 6.3, and about 6 Å for **2**, **3**, and **4**, respectively. In particular, the shortest interguest distance (≈3.1 Å) in **1a**·(**2**)$_2$, between the two oxygen atoms of the nitronyl nitroxide groups, is comparable to the sum of the van der

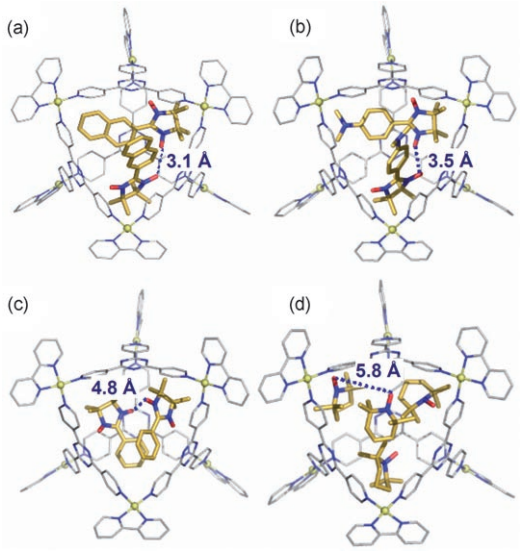

Figure 2. Crystal structures of clathrate complexes a) $\mathbf{1a}\cdot(\mathbf{2})_2$, b) $\mathbf{1b}\cdot(\mathbf{3})_2$, c) $\mathbf{1a}\cdot(\mathbf{4})_2$, and d) $\mathbf{1a}\cdot(\mathbf{5})_4$. Oxygen and nitrogen atoms are colored red and blue, respectively.

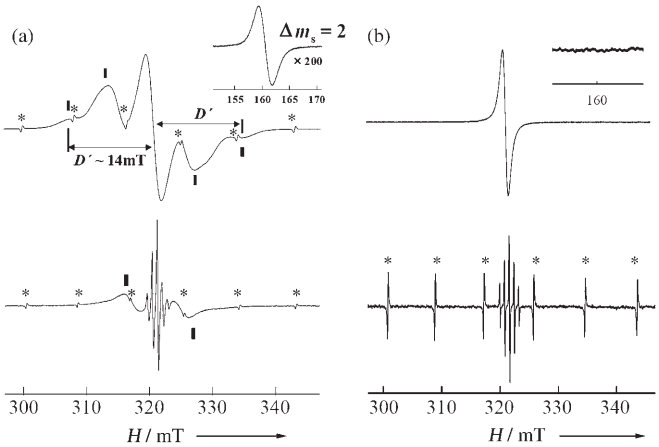

Figure 3. ESR spectra of a) the clathrate compound $\mathbf{1a}\cdot(\mathbf{2})_2$ in powder (top) and 5 mM solution (bottom) and b) the radical **2** in powder (top) and in saturated solution (bottom). Bars indicate signals derived from the triplet state. Asterisks indicate Mn^{2+} external reference.

Waals radii. On the other hand, the radicals themselves take on an antiparallel packing in the guest crystals owing to the bulky methyl groups adjacent to the spin centers, which position the spin centers between radicals far from each other (Figure S2).[12] These results show that the radicals are effectively packed within the cage to interact with each other because of the steric constraints of the cavity.

Cavity-Induced Through-Space Spin–Spin Interaction

ESR studies clarified that $\mathbf{1a}\cdot(\mathbf{2})_2$ has a triplet state in both the solid state and in solution, whereas radical **2** in the absence of cage **1a** always showed a doublet state. In the solid state, $\mathbf{1a}\cdot(\mathbf{2})_2$ showed a split signal at around 320 mT and a signal at a half-field corresponding to a $\Delta m_s = 2$ transition (Figure 3a). Both signals unambiguously prove the triplet state of $\mathbf{1a}\cdot(\mathbf{2})_2$. The distance ($r$) between spin centers was estimated to be 5.8 Å by a point-dipole approximation (in which the split width D' is approximately proportional to $1/r^3$). The estimated distance r corresponds to the observed average distance between the spin centers of the nitronyl nitroxide groups (5.9 Å) determined by X-ray analysis. This result indicates that the triplet state is induced by the intermolecular spin–spin interaction of radicals within the cage.

Signals observed for $\mathbf{1a}\cdot(\mathbf{2})_2$ were broader than those of **2** in the guest crystal because there were several arrangements of radicals in the cage (Figure 3a,b, top), as indicated by the disordered structures in the crystallographic analysis. In contrast with $\mathbf{1a}\cdot(\mathbf{2})_2$, radical **2** in the guest crystal showed a typical doublet signal as expected from the antiparallel packing pattern (Figure 3b). Measurements of the magnetic susceptibility and variable-temperature ESR spectroscopy confirmed that this triplet state is the excited state with an energy difference of 0.6 cm^{-1}, which corresponds to a spin-exchange interaction of $J = -0.3$ cm^{-1} (Figures S3 and S4).

In solution, the ESR spectrum of $\mathbf{1a}\cdot(\mathbf{2})_2$ involves two signals (Figure 3a, bottom). One is a sharp doublet-state signal, which is split into a 1:2:3:2:1 quintet owing to coupling with two nitrogen nuclei ($I=1$). Another is a split broad signal attributed to the triplet state. The triplet-state signal was also observed both in the solid and in frozen solution. This result shows that the radicals can interact with each other even in solution because they are encapsulated and geometrically fixed in the cage. The split width becomes narrower and the signal becomes broader because of a fast exchange between the triplet and the doublet states. On the other hand, radical **2** in the absence of **1a** showed a typical doublet spectrum because there was no particular interaction between radicals (Figure 3b, bottom). The other clathrate compounds, $\mathbf{1b}\cdot(\mathbf{3})_2$, $\mathbf{1a}\cdot(\mathbf{4})_2$, and $\mathbf{1a}\cdot(\mathbf{5})_4$, also showed triplet-state spectra in the solid state (Figure S6). In solution, however, the inductions of the spin–spin interaction of these radicals were weaker than that of $\mathbf{1a}\cdot(\mathbf{2})_2$, because the interaction between radicals **3**, **4**, and **5** and the cages were not so strong and allowed for more opportunities for the radicals to be outside the cage. The triplet signal intensities decreased in the order $\mathbf{1a}\cdot(\mathbf{2})_2$, $\mathbf{1b}\cdot(\mathbf{3})_2$, $\mathbf{1a}\cdot(\mathbf{4})_2$, and $\mathbf{1a}\cdot(\mathbf{5})_4$ (Figure 4).

Relationship between Spin–Spin Interaction and Guest Affinity to the Cage

The quantity of triplet species induced by encapsulation in the cage is expected to correlate with the affinity of the radicals to the cage. We estimated the affinity in solution by cyclic voltammetry (Figures 5 and S7–S9). The guest with a higher affinity to **1a** showed a larger cathode shift in the half-wave potential, $\Delta E_{1/2}^{0/+} = E_{1/2}^{0/+}(\text{clathrated guest}) - E_{1/2}^{0/+}(\text{free guest})$, because it is more shielded by the cage.[13] In fact, radical **2**, which has the highest affinity to **1a** in solu-

CHEMISTRY
AN ASIAN JOURNAL

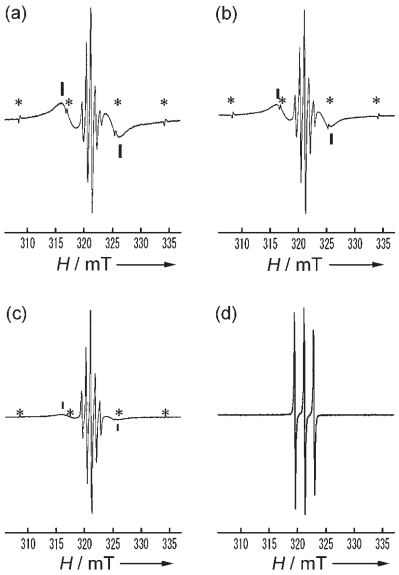

Figure 4. ESR spectra of a) **2** (10 mM), b) **3** (10 mM), c) **4** (10 mM), and d) **5** (10 mM) in the presence of cage **1a** (5 mM) in H_2O. Bars indicate signals derived from the triplet state. Asterisks indicate Mn^{2+} external reference.

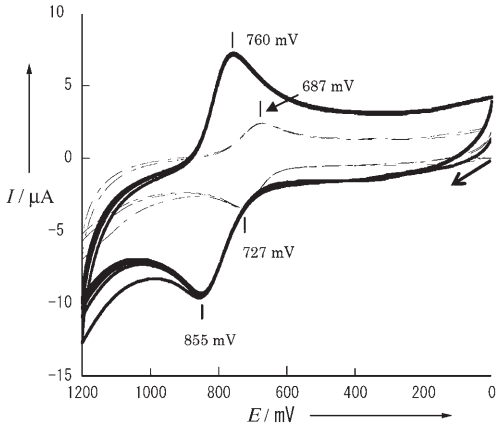

Figure 5. Cyclic voltammograms of radical **2** (1 mM) in the presence of cage **1a** (0.5 mM) (black line) and radical **2** (saturated) (gray dashed line). Scan rate = 100 mV s^{-1} versus Ag^+/AgCl, 30 mM $NaNO_3$.

tion, showed the largest $\Delta E_{1/2}^{0/+}$ value (102 mV). Radical **3** also showed a high affinity ($\Delta E_{1/2}^{0/+} = 68$ mV). The $\Delta E_{1/2}^{0/+}$ values of **4** and **5** were 38 and 2 mV, respectively. The order of the quantity of the triplet-state species estimated by ESR spectroscopy (Figure 4) agreed reasonably with that of the affinity determined by $\Delta E_{1/2}^{0/+}$.

Thermal and pH Control of the Through-Space Spin–Spin Interaction

The through-space spin–spin interaction should be quite sensitive to external stimuli because the radicals are sustained within the cage only by relatively weak hydrophobic forces. Because the affinity between the radicals and the cage is an important factor for controlling the spin–spin interaction as mentioned above, we attempted to manipulate the radical arrangements in the cage with heat or pH. In the case of thermal control, when a solution of **1a**·(**2**)$_2$ was warmed from 103 to 363 K, the split width between the broad signals attributed to the triplet state gradually decreased, because the equilibrium between triplet and doublet states was shifted towards the latter (Figure 6). The frozen solution of

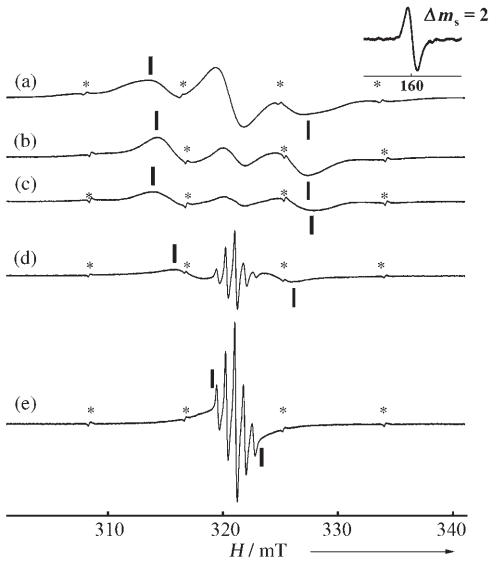

Figure 6. Temperature-dependent ESR spectra of **1a**·(**2**)$_2$ in a) the solid state (top) and b–e) 5 mM solution: b) 103 K (frozen), c) 273 K (frozen), d) 293 K, e) 363 K. Bars indicate signals derived from the triplet state. Asterisks indicate Mn^{2+} external reference.

1a·(**2**)$_2$ gave an ESR spectrum similar to that for the powder owing to a shift of the equilibrium to the triplet state. In solution, however, the interaction became weaker as radicals could move around readily, and the doublet state became more stable. At 363 K, the triplet species was hardly observed. These thermal changes were reversible.

Besides thermal control, we examined pH control of the spin–spin interaction. Radical **3** with a protonation site at the amine group responded to proton concentration in solution, but radical **2**, with no protonation site, did not respond at all.[14] The clathrate compound **1b**·(**3**)$_2$ also showed a typical triplet spectrum at pH 6.5 (Figure 7a). When the solution was acidified to pH 1.3 with HNO_3, the triplet signal disappeared and, instead, a doublet signal appeared with a hyperfine structure due to coupling with the nitrogen nucleus (Figure 7b).[15] When the acidic solution was again adjusted to pH 6.5 with K_2CO_3, the triplet signals reappeared (Figure 7c). These observations suggest that the protonated radical **3**·H^+ was released from the cage in acidic solution, and the released radical was re-encapsulated in the cavity of **1b** by neutralization.

This reversible "release-and-encapsulation" mechanism was confirmed by UV/Vis absorption experiments. The clathrate compound **1b**·(**3**)$_2$ at pH 6.5 showed an n–π^* tran-

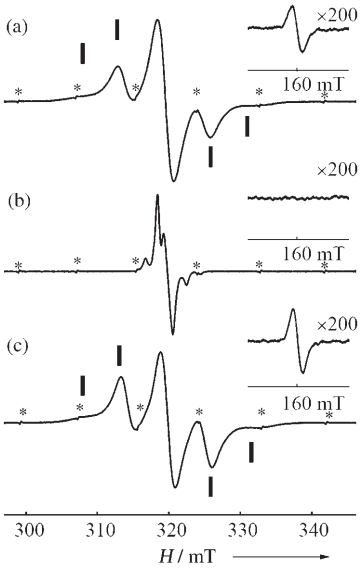

Figure 7. ESR spectra of $\mathbf{1b}\cdot(\mathbf{3})_2$ (0.5 mM, 103 K): a) initial solution (pH 6.5), b) solution acidified with HNO_3 (pH 1.3), c) solution neutralized with K_2CO_3 (pH 6.5). The insets show forbidden transitions. Bars indicate signals derived from the triplet state.[16] Asterisks indicate Mn^{2+} external reference.

sition absorption band at 650 nm accompanied by vibronic coupling derived from **3**, although radicals **3** and $\mathbf{3}\cdot H^+$ in the absence of **1a** in solution showed absorption bands without vibronic coupling at 650 and 560 nm, respectively (Figure 8). Under acidic conditions (pH 1.3), $\mathbf{1b}\cdot(\mathbf{3})_2$ showed absorption bands at both 560 (without vibronic coupling) and 650 nm, suggesting that **3** in **1b** and decapsulated $\mathbf{3}\cdot H^+$ were in equilibrium (Scheme 1). Deconvolution analysis of the spectrum of $\mathbf{1b}\cdot(\mathbf{3})_2$ at pH 1.3 showed a ratio of encapsulated to decapsulated radicals of 3:7 (Figure S13). After neutralization with K_2CO_3, the spectrum obtained was almost identical to the original one at pH 6.5, thus indicating the re-encapsulation of **3** in **1b** (Figure 8a)

Conclusions

We have demonstrated that a self-assembled coordination cage encapsulates stable organic radicals within its hydrophobic cavity and successfully induces through-space spin–spin interaction between the radicals. The salient feature of the coordination cage is the moderate interactions between the host and the guest. Therefore, the spin–spin interaction can be readily manipulated by thermal or pH stimuli reversibly. Our approach, which uses the confined cavity of a self-assembled cage, provides a more-flexible design of spin systems with metal complexes or radicals.

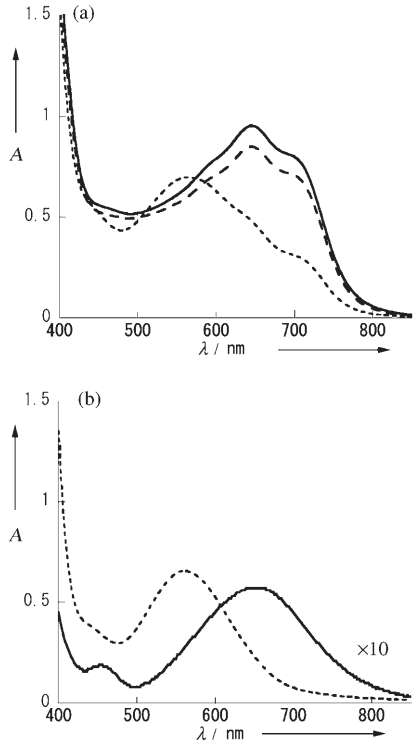

Figure 8. a) UV/Vis spectra of $\mathbf{1b}\cdot(\mathbf{3})_2$ (0.5 mM, 293 K) in solution at pH 6.5 (——), acidified with HNO_3 at pH 1.3 (-----), and neutralized with K_2CO_3 at pH 6.5 (– – –). b) UV/Vis spectra (saturated solution, 293 K) of radical **3** at pH 6.5 (——) and $\mathbf{3}\cdot H^+$ at pH 1.3 (-----).

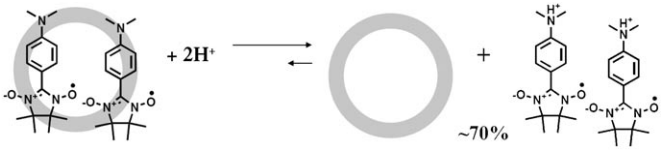

Scheme 1. Equilibrium in a solution (pH 1.3) of $\mathbf{1b}\cdot(\mathbf{3})_2$.

Experimental Section

Materials and Methods

Solvents and reagents were purchased from TCI Co., Ltd., WAKO Pure Chemical Industries Ltd., and Aldrich Chemical, Ltd. and used without any further purification. All ESR spectra were recoded on a JEOL JES-RE1X spectrometer. Mn^{2+} signals as an external standard are indicated in inverse phase on the ESR spectra. The modulation frequency was 100 kHz. ESR spectra in solution were recorded by using a LABOTEC capillary tube, whereas spectra in frozen solution and the solid state were recorded with a quartz tube. All samples were freeze-dried to exclude oxygen before ESR measurements. The *g* values of ESR spectra were as follows: 2.007 ± 1 for **2**, **3**, and **4**, and 2.006 ± 1 for **5** in either the absence or presence of **1**. All UV/Vis spectra were recorded on a SHIMADZU UV-3150 spectrophotometer by using a cell 1 mm wide, except for the spectrum of **2** in H_2O, which was recorded with a cell 1 cm wide (Figure S1). Electrochemical experiments were performed with a BAS100B/W electrochemical analyzer (Bioanalytical Systems). A glassy carbon working electrode (7 mm^2), a Pt counter electrode, and an Ag^+/AgCl reference electrode were utilized in a single-component cell. The working

electrode was polished with 0.05-μm alumina on a felt surface and rinsed with water prior to each measurement. All samples for cyclic voltammetry were bubbled with Ar gas for 15 min to exclude oxygen before measurements.

Syntheses

The preparation of **1a** and **1b** is described in previous reports.[10]

Radical **2** used as the guest was prepared by the improved Ulman procedure.[17] Elemental analysis: calcd (%) for $C_{17}H_{19}N_2O_2$: C 72.06, H 6.76, N 9.89; found: C 71.19, H 6.88, N 9.62.

Radical **3** was prepared by a procedure described previously.[17,18] Elemental analysis: calcd (%) for $C_{15}H_{22}N_3O_2$: C 65.19, H 8.02, N 15.21; found: C 65.06, H 8.16, N 14.99.

1a·(**2**)$_2$: An excess of powdered **2** (5.6 mg, 20 μmol) was suspended in a solution (5 mM) of **1a** (17.8 mg, 5 μmol in 1 mL H_2O) and stirred at 293 K for 1 h. After filtration of surplus **2**, a solution of **1a**·(**2**)$_2$ was obtained. Evaporation of H_2O from the solution gave powdered **1a**·(**2**)$_2$ quantitatively, which was used for ESR measurements. Slow evaporation of water from the aqueous solution of **1a**·(**2**)$_2$ gave single crystals suitable for X-ray diffraction. Elemental analysis: calcd (%) for $C_{166}H_{134}N_{52}O_{40}Pd_6{\cdot}21H_2O$: C 44.17, H 3.93, N 16.14; found: C 44.49, H 4.06, N 15.75.

1b·(**3**)$_2$: In a similar way, **1b**·(**3**)$_2$ was formed quantitatively. Single crystals suitable for X-ray diffraction were obtained by slow evaporation of water from the aqueous solution of the complex. Elemental analysis: calcd (%) for $C_{162}H_{182}N_{54}O_{61}Pt_6{\cdot}21H_2O$: C 38.67, H 3.65, N 15.03; found: C 38.95, H 3.81, N 14.66.

1a·(**4**)$_2$: Two equivalents of **4** (2.3 mg, 10 μmol) were added to a solution (5 mM) of **1a** (17.8 mg, 5 μmol in 1 mL H_2O) and stirred at 293 K for 1 h to produce a solution of **1a**·(**4**)$_2$. Evaporation of H_2O from the solution gave powdered **1a**·(**4**)$_2$ quantitatively, which was used for ESR measurements. Slow evaporation of H_2O from the solution gave single crystals of **1a**·(**4**)$_2$ suitable for X-ray diffraction, quantitatively. Elemental analysis: calcd (%) for $C_{158}H_{130}N_{52}O_{40}Pd_6{\cdot}25\ H_2O$: C 42.30, H 4.04; N 16.24; found: C 42.33, H 3.85, N 16.29.

1a·(**5**)$_4$: Four equivalents of **5** (3.1 mg, 20 μmol) were added to a solution (5 mM) of **1a** (17.8 mg, 5 μmol in 1 mL H_2O) and stirred at 293 K for 1 h to produce a solution of **1a**·(**5**)$_2$. Evaporation of H_2O from the solution gave powdered **1a**·(**5**)$_2$ quantitatively, which was used for ESR measurments. Slow evaporation of H_2O from the solution gave single crystals of **1a**·(**5**)$_4$ suitable for X-ray diffraction, quantitatively. There was a slight difference between the compositions obtained from X-ray and elemental analysis, possibly because of the volatile character of **1a**·(**5**)$_4$. Elemental analysis: calcd (%) for $C_{162.6}H_{157.2}N_{51.4}O_{39.4}Pd_6{\cdot}48\ H_2O$: C 39.33, H 5.14, N 14.50; found: C 39.04, H 4.75, N 14.23.

Crystallography

Single-crystal XRD data for **1a**·(**2**)$_2$, **1b**·(**3**)$_2$, **1a**·(**4**)$_2$, and **1a**·(**5**)$_4$ were collected with a Siemens SMART/CCD diffractometer with $Mo_{K\alpha}$ radiation. The data were corrected for absorption with the SADABS program. SHELXTL-97 was used for structure solution and refinement. Because the guest molecules **2**–**5** showed severe disorder, the geometric parameters were restrained by using those reported previously.[19] As the occupancy factor of the guest molecules settled to about 50%, the value was fixed in the final refinement. The guests and nitrate anions were isotropically refined except for the guest **3**. Non-hydrogen atoms of the cage framework were refined anisotropically, and all hydrogen atoms were fixed at calculated positions and refined with a riding model.

Crystal data for **1a**·(**2**)$_2$: $C_{149}H_{96}N_{48}O_{76}Pd_6$, $M_r = 4413.14$, tetragonal, $P4_32_12$, $a = b = 29.162(3)$, $c = 30.451(6)$ Å, $V = 25896(7)$ Å^3, $Z = 4$, $T = 80(2)$ K, $\rho_{calcd} = 1.132$ g cm^{-3}, λ ($Mo_{K\alpha}$) = 0.71073 Å; 295168 reflections were measured, of which 31871 unique reflections ($R_{int} = 0.2379$) were used in all calculations. The structure was solved by direct methods (SHELXL-97) and refined by full-matrix least-squares on F^2 with 1048 parameters. $R_1 = 0.1504$ ($I > 2\sigma(I)$), $wR_2 = 0.3338$, GOF = 1.045, max./min. residual density = 2.171/−0.899 e Å^{-3}. The details of the refinement are described in a cif file.

Crystal data for **1b**·(**3**)$_2$: $C_{162}H_{140}N_{50.50}O_{80.75}Pt_6$, $M_r = 5256.79$, tetragonal, $P4_12_12$, $a = b = 29.0831(9)$, $c = 30.773(2)$ Å, $V = 26029(2)$ Å^3, $Z = 4$, $T = 90(1)$ K, $\rho_{calcd} = 1.341$ g cm^{-3}, λ ($Mo_{K\alpha}$) = 0.71073 Å; 404871 reflections were measured, of which 40114 were unique ($R_{int} = 0.1341$) and were used in all calculations. The structure was solved by direct methods (SHELXL-97) and refined by full-matrix least-squares on F^2 with 1520 parameters. $R_1 = 0.0716$ ($I > 2\sigma(I)$), $wR_2 = 0.1774$, GOF = 1.011, max./min. residual density = 1.155/−0.831 e Å^{-3}. The detail of the refinement is described in a cif file.

Crystal data for **1a**·(**4**)$_2$: $C_{145}H_{96}N_{50}O_{90}Pd_6$, $M_r = 4617.12$, tetragonal, $P4_32_12$, $a = b = 29.320(4)$, $c = 30.182(6)$ Å, $V = 25947(7)$ Å^3, $Z = 4$, $T = 80(2)$ K, $\rho_{calcd} = 1.182$ g cm^{-3}, λ ($Mo_{K\alpha}$) = 0.71073 Å; 295803 reflections were measured, of which 31506 were unique ($R_{int} = 0.1395$) and were used in all calculations. The structure was solved by direct methods (SHELXL-97) and refined by full-matrix least-squares on F^2 with 1288 parameters. $R_1 = 0.1207$ ($I > 2\sigma(I)$), $wR_2 = 0.2868$, GOF = 1.044, max./min. residual density = 1.206/−1.094 e Å^{-3}. The detail of the refinement is described in a cif file.

Crystal data for **1a**·(**5**)$_2$: $C_{168}H_{96}N_{52.5}O_{77.5}Pd_6$, $M_r = 4728.38$, tetragonal, $P2_12_12_1$, $a = 29.092(6)$, $b = 29.101(6)$, $c = 30.649(6)$ Å, $V = 25947(8)$ Å^3, $Z = 4$, $T = 81(2)$ K, $\rho_{calcd} = 1.210$ g cm^{-3}, λ ($Mo_{K\alpha}$) = 0.71073 Å; 305517 reflections were measured, of which 62935 were unique ($R_{int} = 0.1435$) and were used in all calculations. The structure was solved by direct methods (SHELXL-97) and refined by full-matrix least-squares on F^2 with 2362 parameters. $R_1 = 0.1110$ ($I > 2\sigma(I)$), $wR_2 = 0.2748$, GOF = 1.042, max./min. residual = density 1.106/−1.300 e Å^{-3}. The detail of the refinement is described in a cif file.

Crystal data for **3**: $C_{15}H_{22}N_3O_2$, $M_r = 276.36$, monoclinic, $P2_1/n$, $a = 13.018(2)$, $b = 9.434(1)$, $c = 13.505(2)$ Å, $\alpha = \gamma = 90$, $\beta = 116.840(2)°$, $V = 1479.9(3)$ Å^3, $Z = 4$, $T = 90(1)$ K, $\rho_{calcd} = 1.258$ g cm^{-3}, λ ($Mo_{K\alpha}$) = 0.71073 Å; 5418 reflections were measured, of which 3305 were unique ($R_{int} = 0.0919$) and were used in all calculations. The structure was solved by direct method (SHELXL-97) and refined by full-matrix least-squares on F^2 with 187 parameters. $R_1 = 0.0968$ ($I > 2\sigma(I)$), $wR_2 = 0.2418$, GOF = 1.146; max./min. residual density = 0.870/−0.494 e Å^{-3}. The detail of the refinement is described in a cif file.

CCDC-249974 (**1a**·(**2**)$_2$), -271224 (**3**), and -271223 (**1b**·(**3**)$_2$) contain the supplementary crystallographic data for this paper. These data can be obtained free of charge from the Cambridge Crystallographic Data Centre at www.ccdc.cam.ac.uk/data_request/cif.

[1] a) K. Awaga, Y. Maruyama, *J. Chem. Phys.* **1989**, *91*, 2743–2747; b) S. Nakatsuji, H. Anzai, *J. Mater. Chem.* **1997**, *7*, 2161–2174.

[2] a) K. Matuda, M. Irie, *J. Am. Chem. Soc.* **2000**, *122*, 8309–8310; b) W. Fujita, K. Awaga, *Science* **1999**, *286*, 261–262; c) M. E. Itkis, X. Chi, A. W. Cordes, R. C. Haddon, *Science* **2002**, *296*, 1443–1445.

[3] Through-bond approach: a) A. Rajca, S. Rajca, *J. Am. Chem. Soc.* **1996**, *118*, 8121–8126; b) A. Rajca, S. Rajca, J. Wongsriratanakul, *Science* , **2001**, *294*, 1503–1505; c) R. Ziessel, C. Stroh, H. Heise, F. H. Köhler, P. Turek, N. Claiser, M. Souhassou, C. Lecomte, *J. Am. Chem. Soc.* **2004**, *126*, 12604–12613.

[4] Through-space approach: a) Y. Mazaki, K. Kobayashi, *J. Chem. Soc. Chem. Commun.* **1992**, 1661–1663; b) R. Chiarell, A. Novak, A. Rassat, J. L. Tholence, *Nature* **1993**, *363*, 147–149; c) N. Yoshioka, M. Irisawa, Y. Mochizuki, T. Kato, H. Inoue, S. Ohba, *Chem. Lett.* **1997**, *3*, 251–252; d) Y. Hosokoshi, K. Katoh, Y. Nakazawa, H. Nakano, K. Inoue, *J. Am. Chem. Soc.* **2001**, *123*, 7921–7922; e) K. Das, M. Pink, S. Rajca, A. Rajca, *J. Am. Chem. Soc.* **2006**, *128*, 5334–5335.

[5] a) M. Verdaguer, A. Bleuzen, V. Marvaud, J. Vaissermann, M. Seuleiman, C. Desplanches, A. Scuiller, C. Train, R. Garde, G. Gelly, C. Lomenech, I. Rosenman, P. Veillet, C. Cartie, F. Villain, *Coord. Chem. Rev.* **1999**, *190–192*, 1023–1047; b) J. S. Miller, *MRS Bull.* **2000**, *25*, 60–64.

[6] a) S. Ohkoshi, K. Arai, Y. Sato, K. Hashimoto, *Nat. Mater.* **2004**, *3*, 857–861; b) S. Ohkoshi, K. Hashimoto, *J. Photochem. Photobiol. C*

2001, *2*, 71–88; c) A. Dei, *Angew. Chem.* **2005**, *117*, 1184–1187; *Angew. Chem. Int. Ed.* **2005**, *44*, 1160–1163.

[7] a) G. J. Halder, C. J. Kepert, B. Moubaraki, K. S. Murray, J. D. Cashion, *Science* **2002**, *298*, 1762–1765; b) T. Kusaka, T. Ishida, T. Nogami, *Mol. Cryst. Liq. Cryst. Sci. Technol. Sect. A* **2002**, *379*, 259–264; c) V. Niel, A. L. Thompson, M. C. Muoz, A. Galet, A. E. Goeta, J. A. Real, *Angew. Chem.* **2003**, *115*, 3890–3893; *Angew. Chem. Int. Ed.* **2003**, *42*, 3760–3763; d) Y.-Q. Tian, C.-X. Cai, X.-M. Ren, C.-Y. Duan, Y. Xu, S. Gao, X.-Z. You, *Chem. Eur. J.* **2003**, *9*, 5673–5685; e) D. Maspoch, D. Ruiz-Molina, K. Wurst, N. Domingo, M. Cavallini, F. Biscarini, J. Tejada, C. Rovira, J. Veciana, *Nat. Mater.* **2003**, *2*, 190–195; f) M. Kurmoo, H. Kumagai, S. M. Hughes, C. J. Kepert, *Inorg. Chem.* **2003**, *42*, 6709–6722; g) T. Kashiwagi, S. Ohkoshi, H. Seino, Y. Mizobe, K. Hashimoto, *J. Am. Chem. Soc.* **2004**, *126*, 5024–5025; h) Z.-X. Wang, X.-F. Shen, J. Wang, P. Zhang, Y.-Z. Li, E. N. Nfor, Y. Song, S. Ohkoshi, K. Hashimoto, X.-Z. You, *Angew. Chem.* **2006**, *118*, 3365–3369; *Angew. Chem. Int. Ed.* **2006**, *45*, 3287–3291.

[8] a) D. L. Caulder, K. N. Raymond, *Acc. Chem. Res.* **1999**, *32*, 975–982; b) S. Leininger, B. Olenyuk, P. J. Stang, *Chem. Rev.* **2000**, *100*, 853–908; c) M. Fujita, K. Umemoto, M. Yoshizawa, N. Fujita, T. Kusukawa, K. Biradha, *Chem. Commun.* **2001**, 509–518; d) F. A. Cotton, C. Lin, C. A. Murillo, *Acc. Chem. Res.* **2001**, *34*, 759–771; e) F. Hof, S. L. Craig, C. Nuckolls, J. Rebek Jr., *Angew. Chem.* **2002**, *114*, 1556-1578; *Angew. Chem. Int. Ed.* **2002**, *41*, 1488–1508; f) W. J. Lee, S. Samal, N. Selvapalam, H. J. Kim, K. Kim, *Acc. Chem. Res.* **2003**, *36*, 621–630; g) F. Corbellini, L. D. Costanzo, M. Crego-Calama, S. Geremia, D. N. Reinhoudt, *J. Am. Chem. Soc.* **2003**, *125*, 9946–9947; h) D. Fiedler, D. H. Leung, R. G. Bergman, K. N. Raymond, *J. Am. Chem. Soc.* **2004**, *126*, 3674–3675; i) M. Yoshizawa, M. Tamura, M. Fujita, *J. Am. Chem. Soc.* **2004**, *126*, 6846–6847; j) A. Y. Ziganshina, Y. H. Ko, W. S. Jeon, K. Kim, *Chem. Commun.* **2004**, 806–807.

[9] a) K. Nakabayashi, M. Kawano, M. Yoshizawa, S. Ohkoshi, M. Fujita, *J. Am. Chem. Soc.* **2004**, *126*, 16694–16695; b) K. Nakabayashi, M. Kawano, M. Fujita, *Angew. Chem.* **2005**, *117*, 5456–5459; *Angew. Chem. Int. Ed.* **2005**, *44*, 5322–5325.

[10] a) M. Yoshizawa, T. Kusukawa, M. Fujita, K. Yamaguchi, *J. Am. Chem. Soc.* **2000**, *122*, 6311–6312; b) T. Kusukawa, M. Fujita, *J. Am. Chem. Soc.* **2002**, *124*, 13576–13582.

[11] Delocalization of electrons occurs in the O–N–C–N–O moiety.

[12] We could not determine for certain the configuration of the radicals of **5** within **1a**, because they were highly disordered.

[13] a) T. Matue, D. H. Evans, T. Osa, N. Kobayashi, *J. Am. Chem. Soc.* **1985**, *107*, 3411–3417; b) R. Isnin, C. Salam, A. E. Kaifer, *J. Org. Chem.* **1991**, *56*, 35–41; c) A. E. Kaifer, *Acc. Chem. Res.* **1999**, *32*, 62–71; d) C. M. Cardona, S. Mendoza, A. E. Kaifer, *Chem. Soc. Rev.* **2000**, *29*, 37–42.

[14] ESR spectra of $\mathbf{1b}\cdot(\mathbf{2})_2$ in acidic and neutral solution at 293 K are shown in Figure S10.

[15] ESR spectra of the protonated radical $\mathbf{3}\cdot H^+$ in acidic solution at 103 K are shown in Figure S11.

[16] pH-dependent ESR spectra of $\mathbf{1b}\cdot(\mathbf{3})_2$ at 293 K are shown in Figure S12.

[17] C. Hirel, K. E. Vostrikova, J. Pecaut, V. I. Ovcharenko, P. Rey, *Chem. Eur. J.* **2001**, *7*, 2007–2014.

[18] H. Sakurai, A. Izuoka, T. Sugawara, *J. Am. Chem. Soc.* **2000**, *122*, 9723–9734.

[19] Radical **2**: a) T. Sugano, M. Kurmoo, H. Uekusa, Y. Ohashi, P. Day, *J. Solid State Chem.* **1999**, *145*, 427–442; for radical **3**, see reference [9]; radical **4**: b) A. Zheludev, V. Barone, M. Bonnet, B. Delley, A. Grand, E. Ressouche, P. Rey, R. Subra, J. Schweizer, *J. Am. Chem. Soc.* **1994**, *116*, 2019–2027; radical **5**: c) A. Capiomont, J. Lajzerowicz, J-F. Legrand, C. Zeyen, *Acta Crystallogr. Sect. B* **1981**, *37*, 1557–1560.

Received: August 31, 2006
Published online: December 14, 2006

